Salt body segmentation with dip and frequency attributes

Adam Halpert and Robert G. Clapp

ABSTRACT

Image segmentation can automatically locate salt boundaries on seismic sections, an often time-consuming and tedious task when undertaken manually. However, using a single seismic attribute (usually amplitude) is sometimes insufficient to achieve an accurate segmentation. Since any quantifiable measure may be employed as an attribute for segmentation, exploring other possible attributes is an important step in developing a more robust segmentation algorithm. Dip variability within a seismic section is one attribute with many advantages for segmentation, and experimenting with different methods for calculating dips can yield improved results. Determining the frequency content of a seismic image offers other opportunities for improvement. Specifically, instantaneous frequency shows promise as another attribute for segmentation, while employing a continuous wavelet transform to study envelope amplitude at different frequencies can improve the performance of the amplitude attribute.

INTRODUCTION

Automated image segmentation offers a means of quickly and efficiently delineating salt bodies on seismic images. When adapted for seismic purposes (Lomask, 2007; Lomask et al., 2007), the Normalized Cuts Image Segmentation (NCIS) algorithm (Shi and Malik, 2000) provides a global solution to the salt boundary calculation. This helps overcome some of the weaknesses of other methods, such as local horizon trackers, that can fail when the boundary fades or becomes discontinuous. A global determination of salt boundaries can be especially important for building velocity models in complex areas; in such cases, image segmentation may be employed to automatically build or update velocity models, helping to alleviate a major bottleneck for iterative imaging projects (Halpert and Clapp, 2008).

The NCIS algorithm relies on one or more seismic attributes to segment an image; the most straightforward of these attributes is envelope of the amplitude. Often, this single attribute provides an accurate calculation of the salt boundary. Unfortunately, in some instances a single attribute is insufficient, and the algorithm cannot produce a reasonable result. Here, we demonstrate situations in which a single-attribute segmentation fails. We then explore possibilities for useful attributes other than amplitude, most notably dip and instantaneous frequency. Finally, we discuss an ultimate goal of designing an interpreter-guided multi-attribute segmentation scheme.

ATTRIBUTE-BASED SEGMENTATION

The NCIS algorithm (Shi and Malik, 2000) functions by calculating relationships between individual pixel pairs in an image. For seismic image segmentation, each pixel is compared to a random selection of neighboring pixels (Lomask, 2007), and each pair is assigned a weight value inversely proportional to the likelihood of a salt boundary existing between them. If these weights are placed in a matrix $\mathbf{W}$, a salt boundary path may be calculated via the eigensystem

$$(\mathbf{D} - \mathbf{W})\mathbf{y} = \lambda \mathbf{D}\mathbf{y} \ , \tag{1}$$

where $\mathbf{D}$ is a diagonal matrix whose elements are the sum of each column of $\mathbf{W}$, and λ and $\mathbf{y}$ are an eigenvalue and eigenvector of the system, respectively. Because the smallest eigenvalue will yield only a constant eigenvector, the eigenvector correseponding to the second smallest eigenvalue of the system is used to segment the image. The eigenvector in question ranges in value from -1 to +1 across the estimated boundary path. The image is segmented either by following a constant eigenvector value across the image - usually the zero-value contour; see Lomask (2007) - or by using outside information to follow different eigenvector values across the image (Halpert and Clapp, 2008).

In the examples cited above, the most common measure or attribute used to determine the likely presence of a salt boundary is amplitude of the envelope. For instance, a large amplitude between two pixels suggests a salt boundary is likely, and will result in a relatively small weight assigned to that pixel pair. Amplitude, however, is not the only attribute that can be used for this purpose. In fact, any quantifiable measure that relates to the presence of a salt boundary may be used as an attribute for segmentation.

Limitations of a single attribute

The sources cited above contain several examples of accurate salt boundary picking using only amplitude to segment the image. In some instances, however, such an approach can lead to inaccurate results. Figure 1 shows one such instance. Since the algorithm attempts to find a minimized path across the image, it often tends toward a straight line in areas of uncertainty. In this case, the algorithm incorrectly cuts across a very steep salt canyon in the Sigsbee synthetic model. Even though the outline of the salt top is faintly visible, amplitude information alone is not enough to correctly guide the segmentation process in this instance. This suggests that further information, in the form of attributes other than amplitude, may be an important part of a more robust segmentation algorithm.

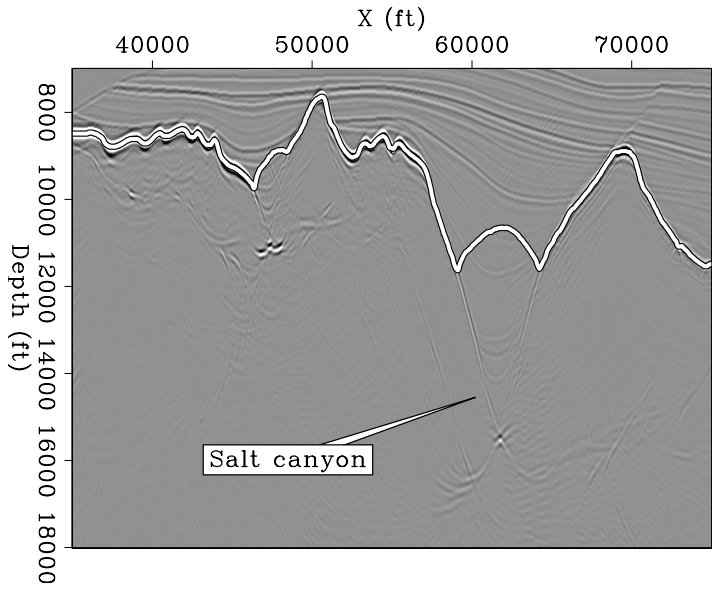

Figure 1: Example of single-attribute segmentation failing to accurately track a salt boundary. The algorithm cuts across the top of the indicated salt canyon. **[CR]**

DIP AS AN ATTRIBUTE

Estimating dip in seismic images has long been recognized as a useful interpretation technique, especially for 3D volumes (Bednar, 1997). Dip can be a particularly useful attribute when the goal is delineation of salt bodies. Lomask (2007) notes that salt boundaries and nearby sediments will often display different dips; furthermore, the seemingly random dips that often characterize the interior of salt bodies on field seismic data should contrast considerably with more ordered dipping layers outside the salt. Therefore, an attribute that highlights variability in dip throughout a seismic image may be helpful for locating salt boundaries.

Dip calculation

Dips on seismic images may be esitmated in several ways. Working from an image processing perspective, van Vliet and Verbeek (1995) describe the process of calculating dips using gradient-square tensors to estimate "orientation" in images. Such methods may easily be adapted to estimate dips of reflectors on seismic images. Claerbout (1992) describes a "plane-wave destructor" mechanism to estimate dips, while Fomel (2002) and Hale (2007) use different plane-wave destructor stencils to implement dip filters. Each of these methods for estimating dips produces a different result, so it is important to determine how these differences can affect the segmentation process.

Figure 2 shows a migrated section of a 2D Gulf of Mexico dataset used for examples throughout this paper; the strong reflector represents the base of a salt body. The

first column of Figure 3 displays dip calculations for the three methods metioned above. Panel (a) is the result of applying Claerbout's "puck" method (Claerbout, 1992), which uses a four-point differencing stencil to calculate directional derivatives. In this example, the random character of dips inside the salt body is readily apparent from the chaotic nature of the dip field, although the boundary itself is difficult to discern. To overcome some of the shortcomings of a four-point stencil, the methods used to obtain the results in panels (b) and (c) instead employ a six-point stencil. The stencil used for panel (b) (Fomel, 2002) is

$$\begin{array}{|c|c|}\hline -\frac{(1+\sigma)(2+\sigma)}{12} & \frac{(1-\sigma)(2-\sigma)}{12} \\ \hline -\frac{(2+\sigma)(2-\sigma)}{6} & \frac{(2+\sigma)(2-\sigma)}{6} \\ \hline -\frac{(1-\sigma)(2-\sigma)}{12} & \frac{(1+\sigma)(2+\sigma)}{12} \\ \hline \end{array}, \tag{2}$$

where σ is the slope of the plane wave being "killed." The stencil used for panel (c) (Hale, 2007) was designed to fit on the previous stencil, while allowing for improved handling of very steep dips. It looks like

$$\begin{array}{|c|c|}\hline -2m^2 & 2mp \\ \hline -4mp & 1 \\ \hline -2p^2 & 2mp \\ \hline \end{array}, \tag{3}$$

where $m = \frac{1}{2}\left[\cos(\tan^{-1}\sigma) + \sin(\tan^{-1}\sigma)\right]$ and $p = \frac{1}{2}\left[\cos(\tan^{-1}\sigma) - \sin(\tan^{-1}\sigma)\right]$. Because of the six-point stencil in use, both methods do a better job of recovering the coherent dips along the salt boundary; panel (c) is the best result, as it performs more accurately even at the steepest dips.

Segmentation using dips

To prepare a dip volume for segmentation, additional steps are necessary. To highlight changes in the dip (an abrupt change is indicative of a salt boundary), a roughener should be applied; here, the helical derivative (Claerbout, 2005) is used to facilitate extension to three dimensions. Finally, calculating the envelope of this volume will produce an image suitable for the segmentation process. The second column of figure 3 shows envelopes for the three dip volumes seen in the left column. Panel (c) shows the clearest salt boundary path, so we expect this image to produce the superior segmentation eigenvector. Figure 4, which displays segmentation results - eigenvectors in the left column, and the corresponding zero-contour boundaries on the right - confirms this expectation. The eigenvector in panel (c) shows the clearest transition from light to dark along the boundary. Panel (b) is skewed by a strong anomaly in the upper left, and panel (a) rarely exhibits a clearly defined boundary. The corresponding zero-contour boundary picks shown in the second column differ greatly in terms of accuracy. Clearly, using Hale's stencil as part of a dip attribute segmentation algorithm produces the most accurate result in this case.

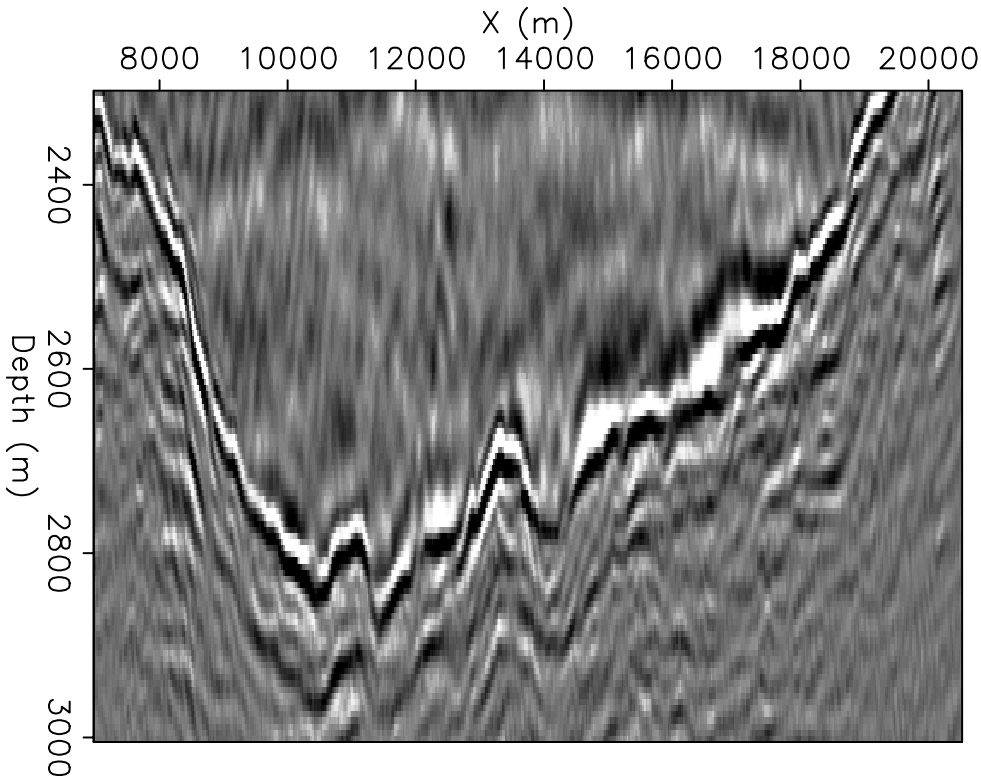

Figure 2: A 2D seismic section used throughout this paper. The strong reflector is the base of a salt body. [**ER**]

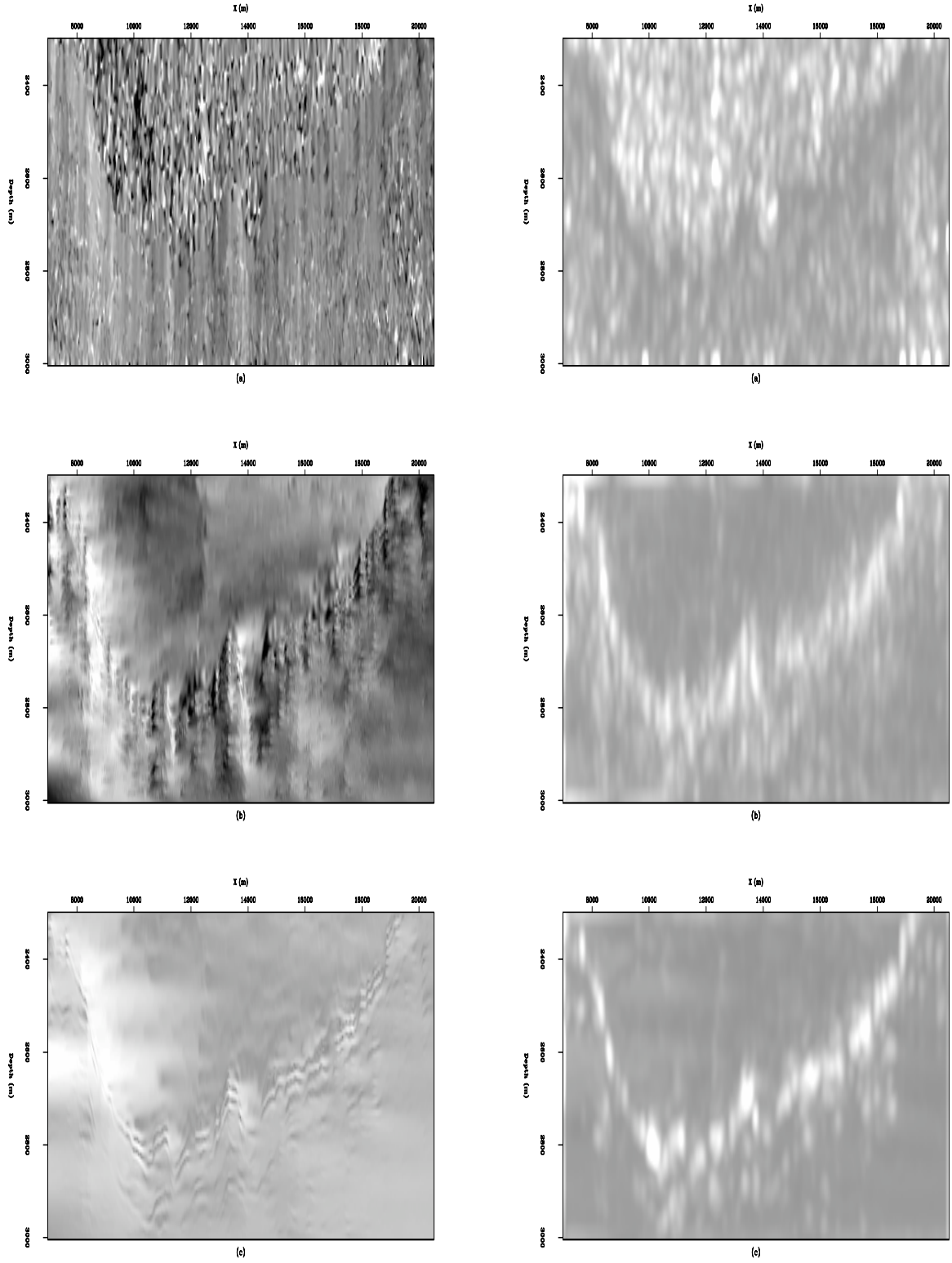

Figure 3: Dip calculations (left column) and their corresponding envelope volumes (right column) for the section in Figure 2. Row (a) uses Claerbout's puck method, row (b) uses Fomel's plane-wave destruction filtering stencil, and row (c) uses Hale's filtering stencil. **[ER]**

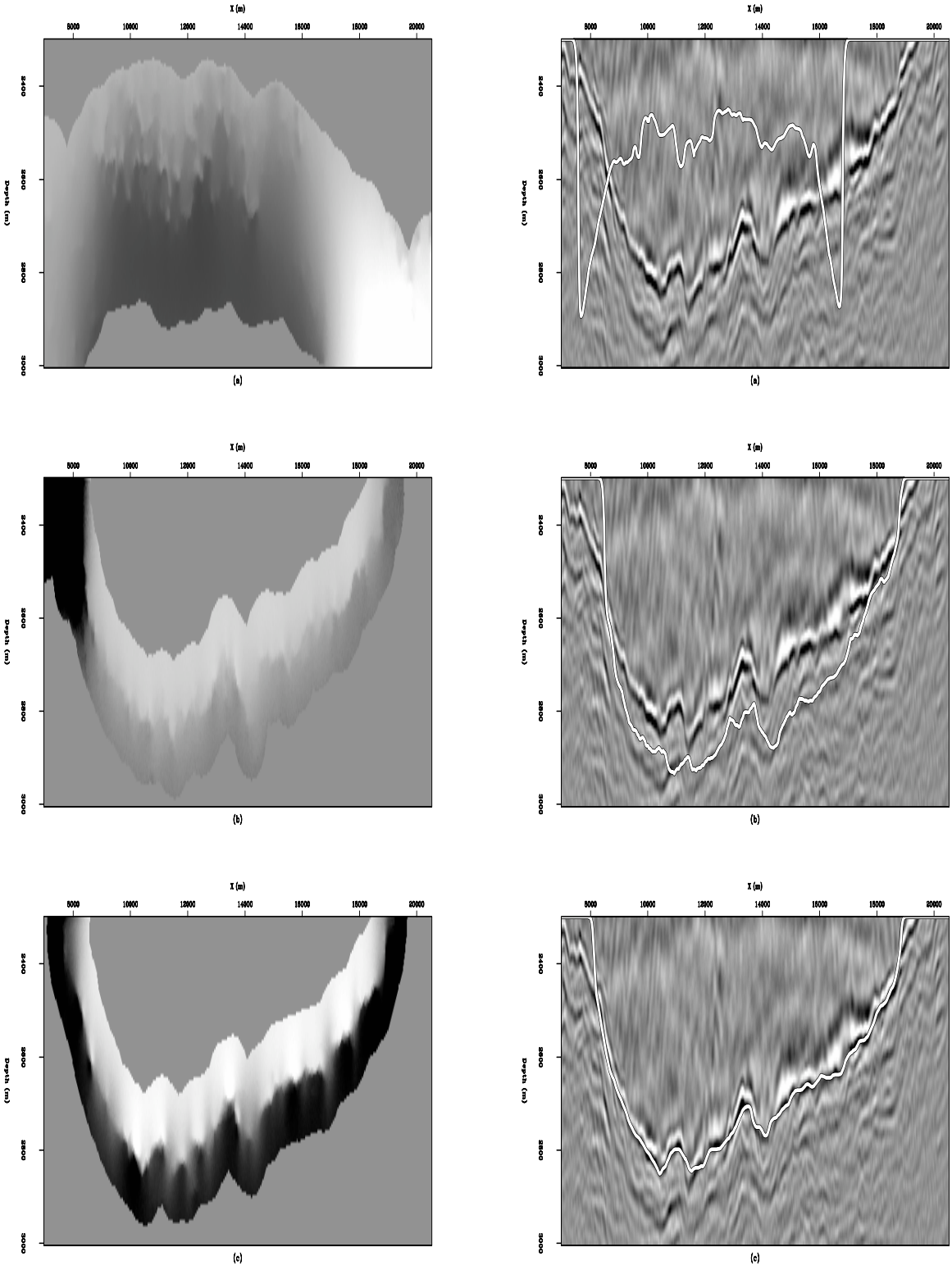

Figure 4: Eigenvectors (left column) and zero-contour boundaries (right column) derived from the dip envelope volumes in Figure 3. [**CR**]

FREQUENCY AS AN ATTRIBUTE

Seismic waves behave differently inside salt bodies than they do when traveling through sediment layers. One way to take advantage of this fact is to calculate *instantaneous frequency* (Taner et al., 1979) in different parts of an image. In the complex representation of a seismic trace

$$A(t)e^{i\phi(t)}, \tag{4}$$

$A(t)$ is the amplitude of the envelope (the most common segmentation attribute), and $\phi(t)$ is the instantaneous phase. The first derivative of the instantaneous phase yields instantaneous frequency. A rapid change in instantaneous frequency may be indicative of a salt boundary, especially if it occurs in a coherent manner across an image. Figure 5 shows the instantaneous frequency calculation for the same 2D section used previously. It is apparent that frequency behavior inside the salt differs noticeably from behavior outside the salt. An eigenvector and boundary derived from this volume can be seen in Figure 6.

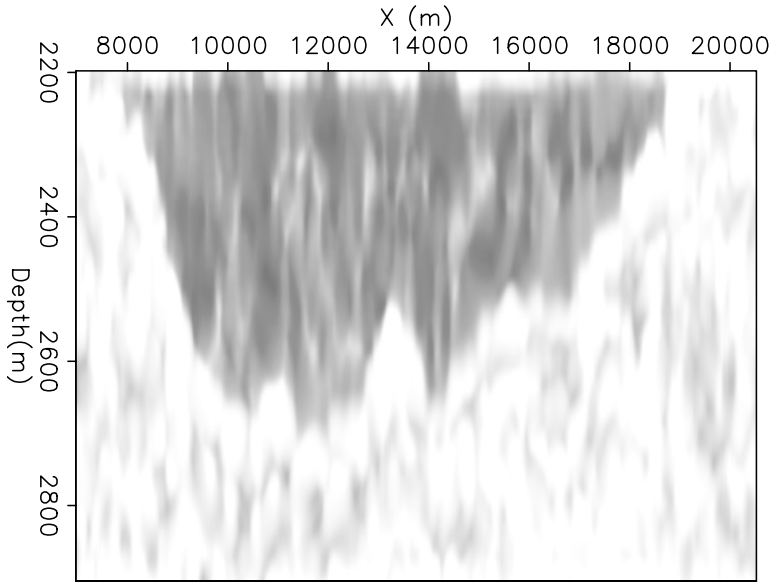

Figure 5: Instantaneous frequency calculation for the seismic section. There is a clear difference in character inside and outside the salt body. [**ER**]

Continuous wavelet transform

Another method for investigating frequency properties of an image is to employ the continuous wavelet transform (Sinha et al., 2005), or CWT, to explore an image's "response" to different frequencies. Because the interior of salt bodies is often characterized by random, high-frequency noise, one application of the CWT is to improve the effectiveness of the *amplitude* attribute by eliminating this noise, thereby emphasizing the amplitude contributions of the salt boundary. Figure 7 compares envelope

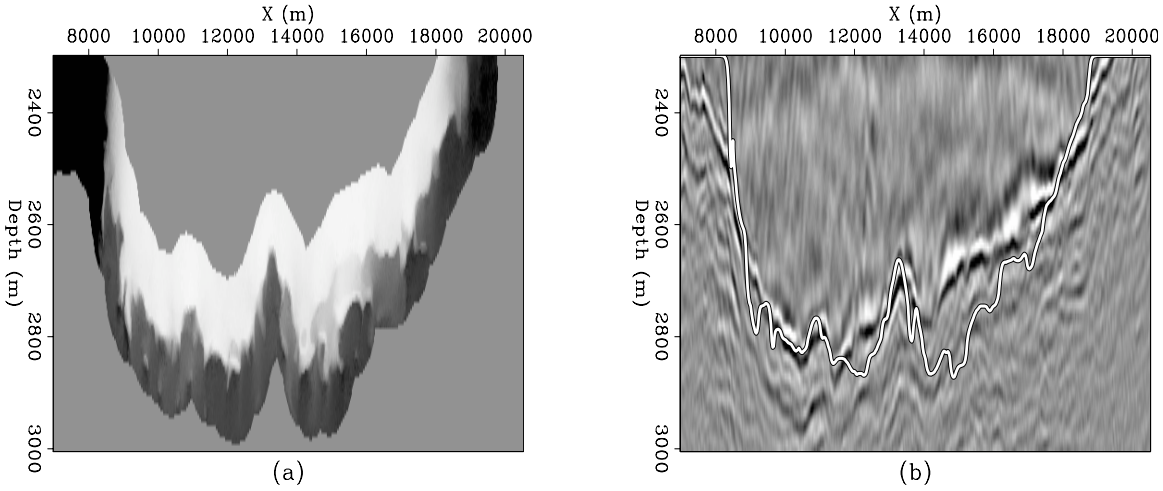

Figure 6: Eigenvector (a) and boundary calculation (b) using the instantaneous frequency attribute from Figure 5. **[CR]**

amplitudes for both the original seismic section in panel (a), and for the same section after a CWT has been used to isolate and stack over only the low frequencies in panel (b). The right-hand image features a much clearer boundary path, and less "noise" both inside and outside the salt body. Such an image allows for an easier segmentation process with less uncertainty.

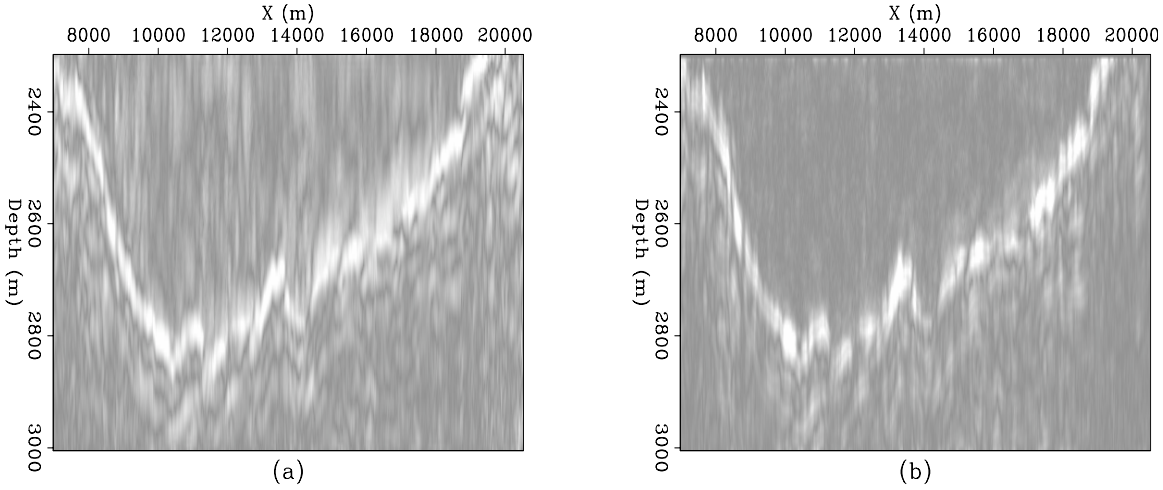

Figure 7: Amplitude envelope when all frequencies are included (a), and after a CWT is used to isolate and stack over only low frequencies (b). **[ER]**

TOWARD MULTI-ATTRIBUTE SEGMENTATION

As a way of comparing segmentation results from different attributes, Figure 8 displays three boundaries overlain on the seismic section. Each boundary is the result

of segmenting with a different attribute: amplitude of the envelope, dip (from Hale's filtering stencil), or instantaneous frequency. Clearly, the results using amplitude and dip are extremely similar, and both closely track the strong reflector known to be the salt base across nearly the entire image. The amplitude boundary is more accurate in the upper left corner, while the dip boundary appears to follow a more likely path at around $x = 17000m$. This result suggests that these attributes can function either independently, or more importantly, in a complementary manner if used together in a multi-attribute segmentation scheme. While the boundary obtained using the instantaneous frequency attribute does not as accurately track the salt interface at all points of the image, it does seem to provide some useful information that may also be important in such a scheme.

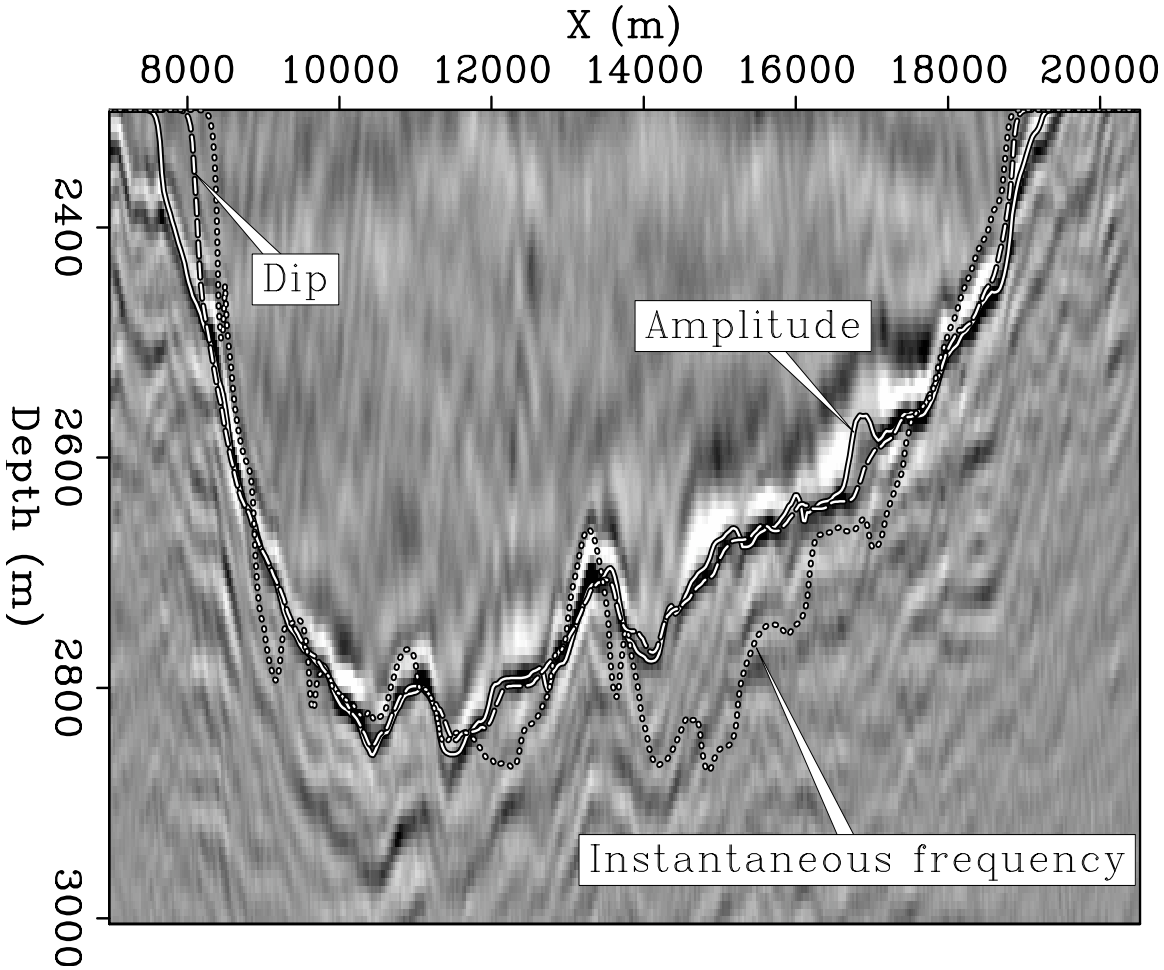

Figure 8: A comparison of boundaries calculated using three different attributes: envelope amplitude (solid line), dip from Hale's filtering stencil (dashed line), and instantaneous frequency (dotted line). **[CR]**

Interpreter-guided segmentation

The purpose of this area of research is to find multiple attributes that may be useful for seismic image segmentation. This raises the important question of how to determine which attribute(s) should be used for segmentation when several are available, especially since not all attributes may be appropriate for a given situation. Here, a human interpreter's input is vital to the process. An ultimate goal for seismic image segmentation is to create an algorithm that can "learn" from the interpreter. For example, if the interpreter picks salt boundaries on a small number of 2D lines from a 3D survey, an inversion algorithm could determine which specific attributes were most important for the manual interpretation. Once this determination is made, the entire 3D volume could be segmented based on the information provided by the human interpreter. This scheme would take advantage both of humans' abilities to accurately pick boundaries on 2D sections, and computers' superior abilities to "see" in three dimensions.

CONCLUSIONS

Amplitude is only one possible seismic attribute that may be used for image segmentation. Because the NCIS algorithm does not always succeed using amplitude alone, other attributes are necessary to achieve higher accuracy. One such attribute is dip; both the nature of salt boundaries and random character of salt body interiors on seismic data make the dip variability attribute useful for segmentation. Frequency content of an image is another important attribute; calculating instantaneous frequencies throughout an image shows promise as a boundary-detection technique. Examining wavelet properties via a continuous wavelet transform also yields potentially useful information for segmentation, especially when used in combination with other attributes like amplitude of the envelope. Ultimately, these attributes could be an important part of an interpreter-aided seismic segmentation algorithm that robustly and accurately picks salt boundaries on 3D seismic volumes.

ACKNOWLEDGMENTS

We would like to thank SMAART JV for the Sigsbee synthetic dataset, and WesternGeco for providing the real data example in this paper.

REFERENCES

Bednar, J. B., 1997, Least squares dip and coherency attributes: SEP-Report, **95**, 219–225.

Claerbout, J., 1992, Earth soundings analysis: Processing versus inversion: Blackwell Scientific Publications.

———, 2005, Image estimation by example: Stanford University.

Fomel, S., 2002, Applications of plane-wave destruction filters: Geophysics, **67**, 1946–1960.

Hale, D., 2007, Local dip filtering with directional laplacians: CWP-Report, **567**.

Halpert, A. and R. G. Clapp, 2008, Image segmentation for velocity model construction and updating: 2008, **134**, 159–170.

Lomask, J., 2007, Seismic volumetric flattening and segmentation: PhD thesis, Stanford University.

Lomask, J., R. G. Clapp, and B. Biondi, 2007, Application of image segmentation to tracking 3d salt boundaries: Geophysics, **72**, P47–P56.

Shi, J. and J. Malik, 2000, Normalized cuts and image segmentation: Institute of Electrical and Electronics Engineers Transactions on Pattern Analysis and Machine Intelligence, **22**, 838–905.

Sinha, S., P. S. Routh, P. D. Anno, and J. P. Castagna, 2005, Spectral decomposition of seismic data with continuous-wavelet transform: Geophysics, **70**, P19–P25.

Taner, M. T., F. Koehler, and R. E. Sheriff, 1979, Complex seismic trace analysis: Geophysics, **44**, 1041–1063.

van Vliet, L. J. and P. W. Verbeek, 1995, Estimators for orientation and anisotropy in digitized images, *in* Proceedings, Conference of the Advanced School for Computing and Imaging, 442–450.